Int J Appl Earth Obs Geoinformation 82 (2019) 101925

Contents lists available at ScienceDirect

Int J Appl Earth Obs Geoinformation

journal homepage: www.elsevier.com/locate/jag

Evaluation of subsidence induced by long-lasting buildings load using InSAR technique and geotechnical data: The case study of a Freight Terminal (Tuscany, Italy)

Andrea Ciampalini[a,*], Lorenzo Solari[b], Roberto Giannecchini[a], Yuri Galanti[a], Sandro Moretti[b]

[a] Dipartimento di Scienze della Terra, Università di Pisa, 56126, Pisa, Italy
[b] Dipartimento di Scienze della Terra, Università degli Studi di Firenze, Via G. La Pira,4, 50121, Firenze, Italy

ARTICLE INFO

Keywords:
Subsidence
InSAR data
Geotechnical data
Compressibility
Consolidation process
Tuscany

ABSTRACT

This paper shows the results of the comparison between Multi-temporal Synthetic Aperture Radar (MTInSAR) products derived from different sensors (C-band ERS 1/2, Envisat, Sentinel-1 and X-band COSMO-SkyMed) and geotechnical data to investigate the driving factors of subsidence which affect a freight terminal located along the a coastal plain of Tuscany (central Italy). MTInSAR data have been acquired in a very long period, between 1992 and 2018 and were analyzed in terms of subsidence rates and deformation time series at building scale. The obtained results show that the oldest buildings are still affected by a deformation rate close to −5 mm/yr, whereas recent buildings register rates around −40 mm/yr. Time series of deformation suggest that the deformation rates decrease over time following time-dependent trend that approximates the typical consolidation curve for compressible soils. The geotechnical and stratigraphical analysis of the subsurface data (boreholes, cone penetration tests and dilatometer tests) highlights the presence of a 15 m thick layer formed of clay characterized by poor geotechnical characteristics. The comparison among InSAR data, subsurface geological framework and geotechnical reconstruction suggests a possible evaluation of the timing of the primary and secondary consolidation processes.

1. Introduction

Anthropogenic subsidence is a major threat in urban areas, resulting in long-term economic losses, sometimes causing inundation and increased flooding potential (Holzer and Johnson, 1985; Shirzaei and Bürgmann, 2018). In particular geological environments, subsidence can create severe damage when differential settlements are realized without suitable foundation apparatus, leading to structures tilting and underground utilities interruption (Peduto et al., 2017). Direct and indirect effects of subsidence generate costs of billion dollars in several coastal cities worldwide (Bucx et al., 2015).

From this point of view, building scale analyses at city scale are required to measure ongoing ground motions. Multi-temporal Synthetic Aperture Radar (MTInSAR) techniques can support this activity, providing a high density of measurement points and long time series of deformation to back-analyze current phenomena (Cigna et al., 2015). Urban areas affected by subsidence are perfect targets for MTInSAR analysis for two main reasons. The first one is the type of movement; as it is well known, radar interferometry cannot measure fast rates above the quarter of wavelength over the revisit interval without encompassing phase unwrapping errors (Zhou et al., 2009). The second reason is related to the radar coherence, thanks to the high density of buildings and infrastructures, urban areas can provide a significant amount of "radar friendly" targets (i.e. Persistent Scatterers, PS), especially when X band radar images are analyzed (Bonano et al., 2013).

The potential of MTInSAR techniques has been widely exploited for subsidence monitoring, focusing on building-scale analyses. This type of approach has been followed by several authors, proposing interesting results such as in Italy (Cigna et al., 2014; Bianchini and Moretti, 2015; Solari et al., 2016, 2017; Bozzano et al., 2018), China (Zhu et al., 2018), Romania (Armaş et al., 2017), Spain (Herrera et al., 2010; Bru et al., 2017) and the Netherlands (Peduto et al., 2017). In particular, MTInSAR results have been used for multiscale subsidence mapping in urban areas, shifting from the city scale, where the area with the highest deformation rates are highlighted, to the building/single infrastructure scale (i.e. Cigna et al., 2014; Solari et al., 2017). MTInSAR

* Corresponding author.
E-mail addresses: andrea.ciampalini@unipi.it (A. Ciampalini), lorenzo.solari@unifi.it (L. Solari), roberto.giannecchini@unipi.it (R. Giannecchini), yuri.galanti@unipi.it (Y. Galanti), sandro.moretti@unifi.it (S. Moretti).

https://doi.org/10.1016/j.jag.2019.101925
Received 12 February 2019; Received in revised form 9 July 2019; Accepted 10 July 2019

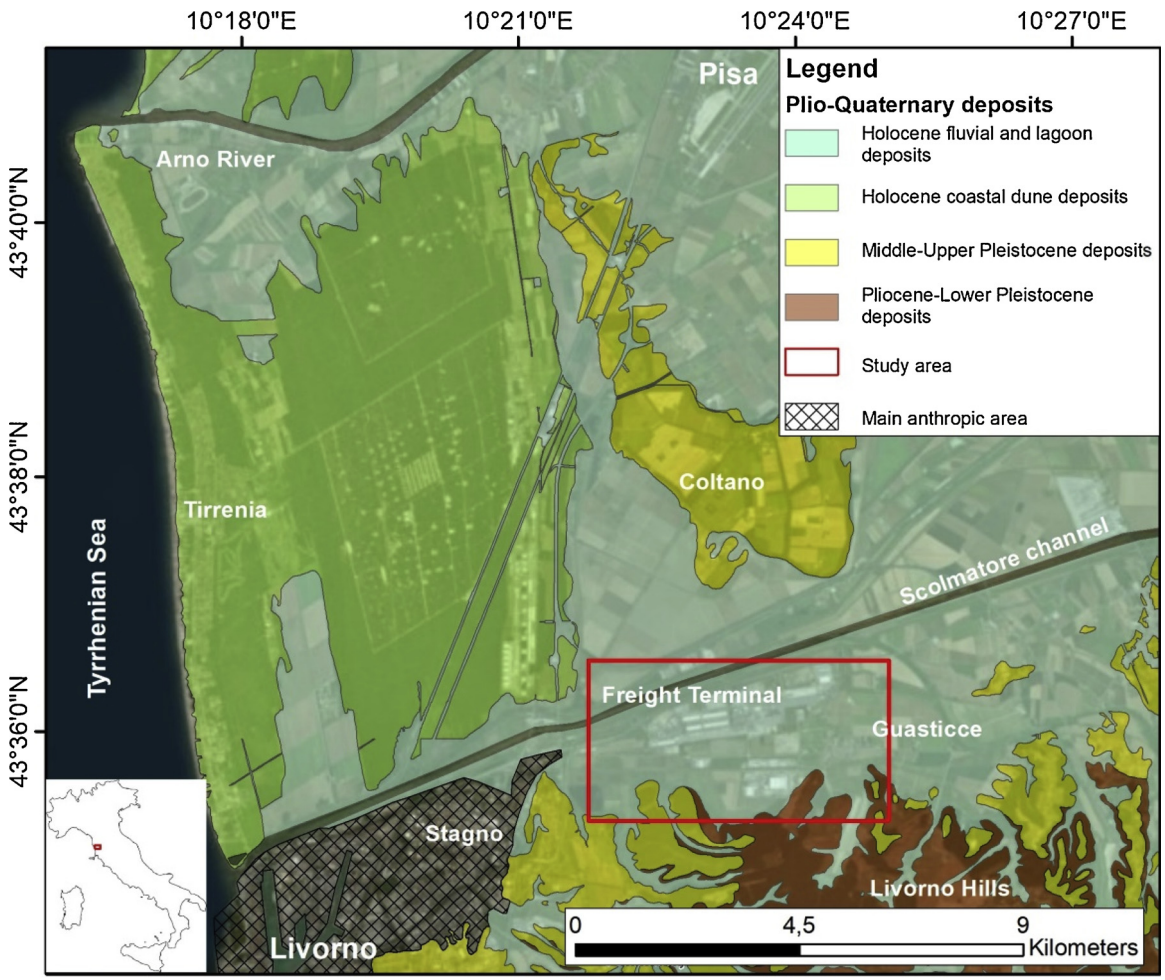

Fig. 1. Location of the study area (red rectangle) with the main geological features. (For interpretation of the references to colour in this figure legend, the reader is referred to the web version of this article).

data have been exploited to reconstruct the long term evolution of subsidence by comparing geological models, derived from borehole information, recorded velocities and building age of construction (Solari et al., 2016; Bozzano et al., 2018). Interferometric data have also been used for structural analysis, deriving fragility curves for buildings with different types of foundations (Peduto et al., 2017). Recently, Zhu et al. (2018) developed an automated procedure to analyze the temporal and spatial behavior of PS points to highlight anomalous trends within large interferometric datasets derived over large urban areas.

In this work, an integrated approach based on multi-band and multi-temporal interferometric results, subsurface stratigraphical, optical imagery (Google Earth and aerial images) and geotechnical data and recent urban development reconstruction is presented. In particular, we used ERS 1/2 (C-band) for the period 1992–2000, Envisat (C-band) for 2003–2010, COSMO-SkyMed (X-band) for 2011–2014 and Sentinel-1 (C-band) for the period 2015–2018). The trend of a representative time series of deformation have been compared with a consolidation curve modeled considering the geotechnical parameters (Hu et al., 2017). This methodology aims at analyzing the 26 years long subsidence of a recently built freight terminal (Guasticce terminal) in the Tuscany Region (Central Italy), at the border between Livorno and Pisa provinces. This area, composed of several commercial sheds and the connected road network, is the main container freight station for the Livorno Port. The Guasticce terminal is affected by subsidence since its construction, dated back to late '80 s; the ground lowering slowly induced structural damage to the sheds, leading to long-term economic losses for the shipping companies working there. The proposed approach has been used to demonstrate the direct relation between urbanization, geotechnical properties of soils and interferometric-based deformation measurements, with a focus on the multi-temporal evolution of recorded subsidence rates.

2. Study area

The Guasticce plain is located in the western part of the Tuscany Region (Fig. 1), along the Tyrrhenian coast and close to the southern boundary of the Arno River valley, which is represented by the Livorno Hills and corresponds to the NE-SW Livorno-Sillaro transversal fault (Ghelardoni et al., 1965; Cantini et al., 2001). The study area is bounded by Holocene coastal dune deposits to the west and by the Livorno Hills to the south, formed of Neogene to Quaternary deposits (Sarti et al., 2015). To the north, the Guasticce area is separated from the main alluvial plain of the Arno River by a morphological relief (Coltano in Fig. 1) rising up to 15 m above the sea level and made of silty sand deposits of uncertain age (Sarti et al., 2015). The upper part of the Arno River coastal plain is filled by an alternation of 100 m of continental and coastal marine deposits cut by two 30 m deep incised-valley systems filled by a fining upward stratigraphic sequence. This sequence is overlaid by a highly compressible silty clay layer, 5 to 15 m thick, deposited within a coastal lagoon. This layer lies beneath a fluvio-deltaic succession, 10–15 m thick, made of clay and silt with lenses of sand (Aguzzi et al., 2007; Sarti et al., 2015).

In correspondence with the main alluvial coastal plains, the coast of

Fig. 2. Examples of damages induced by the subsidence in the of the freight terminal area.

Table 1
Dates of acquisition of the very-high resolution images from Google Earth.

Image number	Acquisition date
1	26/02/2002
2	31/01/2004
3	05/01/2006
4	02/07/2010
5	14/09/2010
6	28/10/2010
7	08/04/2011
8	16/04/2011
9	27/03/2012
10	20/07/2012
11	11/08/2013
12	28/08/2015
13	08/08/2016
14	11/03/2017

the Tuscany is affected by natural subsidence linked to the natural sediment compaction. In particular, the sector of the Versilia-Pisan plain, which includes the Arno River coastal plain, is characterized by an average rate of −0.57 mm/yr (Nisi et al., 2003).

Today, the area close to the village of Guasticce, between the Livorno Hills and the Scolmatore channel, hosts a freight terminal (3,000,000 m^2 wide), built up starting from the 2000. The choice of this area was decided for its strategic position (about 6 km far from the Livorno commercial port) and for the transportation network (proximity to highways and railways). The freight terminal includes several warehouses with an extension varying between 10,000 and 17,000 m^2 and a height between 12 and 14 m above the ground and several loading areas (about 500,000 m^2), where about 1300 heavy trucks per day load and unload goods. Most of the buildings included in the area of the freight terminal clearly show the evidences (cracks and damage) related to fast subsidence phenomena linked to the peculiar subsurface geological framework (Fig. 2).

3. Materials and methods

The proposed approach uses both optical and radar satellite data. In particular, optical images have been used to map all the buildings included in the study area and its urban evolution over time. Space-borne radar data have been used to measure buildings deformation rates in the last 26 years. The integration of these datasets with the available geotechnical data allowed to analyze the consolidation processes of the clay layer as consequence of the buildings load. The complete procedure is described below.

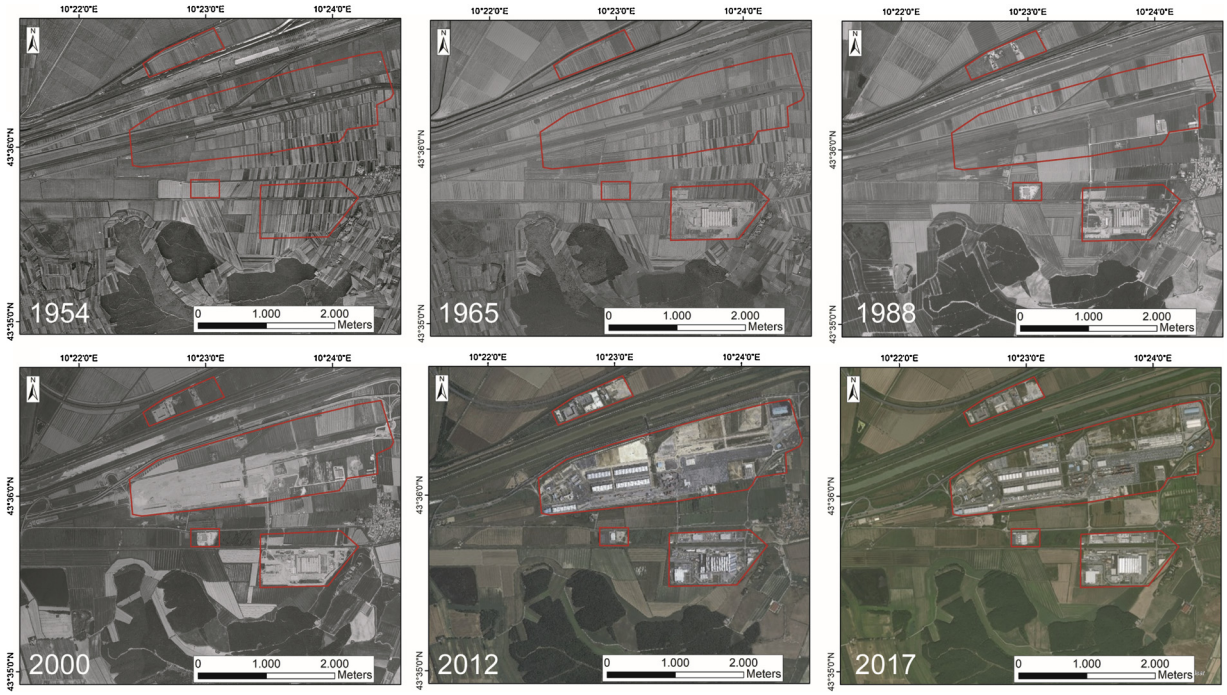

Fig. 3. Examples of orthophotos (1954, 1965, 1988, 2000, 2012) and Google Earth (2017 images used to infer the age of construction of the analyzed buildings. The red polygons correspond to the area occupied today by the freight terminal. (For interpretation of the references to colour in this figure legend, the reader is referred to the web version of this article).

Table 2
Classes identified on the basis of the available optical imagery and acquisition periods of SAR sensors.

Class	Sensor	Period
1	Pre-ERS 1/2	1954–1991
2	ERS 1/2	1992–2001
3	Envisat	2002–2010
4	CSK	2011–2014
5	Sentinel-1	2015–2018

3.1. Buildings map

This step is based on the exploitation of the available optical data to produce a multi-temporal map of buildings included in the study area and to retrieve their age of construction with an approximation of some years depending on the orthophoto temporal coverage. For this purpose, several sources have been queried: i) the WMS (Regione Toscana, Web Map Service, http://www502.regione.toscana.it/wmsraster/com.rt.wms. RTmap/wms?map = wmsofc&map_resolution = 91&language = ita&) of the Tuscany Region, which includes the orthophotos acquired in 1954, 1965, 1978, 1988, 1996, 2000, 2001, 2003, 2005, 2007, 2010, 2012 and 2013; ii) Google Earth, which includes the very high resolution images listed in Table 1. The spatial resolution of the optical images varies between 0.50 m of the Google Earth imagery and 0.20 m of the orthophoto of the Tuscany Region.

The map of the buildings has been produced using the most recent available image (11/03/2017). All the visible buildings have been digitized into a polygonal ESRI shapefile. The images from 1954 to 2017 have been used to infer the age of construction of the buildings included in the study area (Fig. 3).

Considering the available images and the acquisition period of the used SAR sensors, 5 classes have been identified (Table 2). Theses time intervals have been decided on the basis of the acquisition periods of the SAR sensors.

3.2. PSI technique

The PSI (Persistent Scatterer Interferometry) technique is a relatively recent approach that exploits phase information to measure ground deformation (Ferretti et al., 2001; Crosetto et al., 2016). Persistent Scatterers (PS) are point-wise targets characterized by stable radiometric behavior over time. They usually are natural (e.g. rocky outcrops) or man-made (buildings, infrastructures) structures (Crosetto et al., 2016). Phase information backscattered from PS points can be used to retrieve ground displacements during the acquisition period. This technique is particularly effective in urbanized areas, where man-made highly reflective targets are dense (Ciampalini et al., 2014; Jones et al., 2016). Ground deformation is measured along the satellite Line of Sight (LOS) which forms an angle with the topography. In case of flat areas, affected by subsidence, the measured deformation along the LOS can be assumed as vertical (Solari et al., 2018). SqueeSAR (Ferretti et al., 2011) is one of the most recent advanced multi-temporal technique which exploits both Permanent Scatterer (PS) and Distributed Scatterer (DS) which correspond to homogeneous areas spread over a group of pixels in a SAR image (shrubs, rangeland, etc.), increasing the point target density with respect to the PSI technique (Ferretti et al., 2011). Among the information that can be obtained for each measurement point (PS or DS) the most important are: the displacement rate (mm/yr), measured along the LOS and the time series of deformation. Both the deformation time series and displacement rate are differential measurements with respect to a reference point considered stable (Ciampalini et al., 2016; Raspini et al., 2018). The reference point is selected considering different characteristics related to both the radar signal and the geological framework. The reference points are selected considering: (1) geology (e.g., lithology); (2) available thematic maps (e.g., landslide inventory maps, maps of regional or local subsidence) and (3) any prior information about land motion coming from different monitoring systems (e.g., previous InSAR data, GNSS, etc.).

In order to evaluate subsidence phenomena in the study area, ERS 1/2, Envisat, COSMO-SkyMed and Sentinel-1 data have been exploited

Table 3
Characteristics of the available SAR datesets. All the datasets have been acquired in descending orbit.

Satellite	Acquisition period	N° of images	Velocity standard deviation (mm/yr)	Maximum subsidence rate (mm/yr)	Maximum uplift rate (mm/yr)	N° of PS	Incidence angle range (°)	Ground resolution (m)
ERS 1/2	13/05/1992 – 10/12/2000	70	± 0.4	−21.3	3.7	71	23°	26 × 30
Envisat	25/01/2003 – 12/06/2010	37	± 0.5	−20.4	1.4	494	15°-45°	28 × 28
CSK	21/05/2011 – 10/03/2014	47	± 0.3	−39.8	5.6	5730	22°-37°	3 × 3
Sentinel-1	22/03/2015 – 10/02/2018	113	± 0.3	−37	3.2	241	29°-46°	14 × 5

(Table 3). In particular, ERS 1/2, Envisat and COSMO-SkyMed data have been processed with the PSInSAR technique (Ferretti et al., 2001), whereas Sentinel-1 data have been processed with the SqueeSAR technique (Ferretti et al., 2011). ERS 1/2, Envisat and COSMO-SkyMed data were obtained from the National Cartographic Portal (2019) (http://www.pcn.minambiente.it/viewer/) of the Pst-A Project (Piano Straordinario di Telerilevamento). For an explanation of the processing strategies adopted for processing the whole Italian territory we refer to Costantini et al. (2017). Sentinel-1 data have been obtained within the project "Monitoring ground deformation in the Tuscany Region with satellite radar data" funded by the Tuscany Region (https://geoportale.lamma.rete.toscana.it/difesa_suolo/#/viewer/openlayers/326). For further information about how the Sentinel-1 images have been processed by means of the SqueeSAR approach we refer to Raspini et al. (2018). The related maps are reported in Figs. 4. Each datasets is characterized by a different reference point because the data were processed at the regional scale in the framework of different projects and in different periods. The results of these projects are available in their dedicated web portal. They are considered reliable by both the scientific community and the civil protection and local authorities which routinely use them to manage the territory.

Each building polygon is associated with an average LOS deformation velocity for each satellite dataset, taking into account the different point density. The average LOS velocity has been calculated for each SAR dataset to evaluate the subsidence evolution in different periods. Around each polygon a 2-m-wide buffer has been created to: (i) limit problems related to a possible shift between the different layers (buildings and PSI data) and to possible georeferencing error of each PS/DS point (Pratesi et al., 2015); (ii) to limit the effect of the back-scattered signal due to the structure itself (Bianchini et al., 2015) and (iii) increase the number of available PS/DS (Ciampalini et al., 2014). In order to evaluate the LOS deformation velocity of a single building, Pratesi et al. (2015, 2016) suggest to use a buffer with a rate commensurate with the spatial resolution of the SAR images (e.g. 30 m for ERS 1/2 and Envisat data). In the freight terminal the warehouses are very close each other and we think that 30 m is too much; for this reason a 2-m-wide buffer has been arbitrarily used. Thus, the average LOS velocity is the results of the average of all the measurement points located inside each polygon and those located in a neighborhood of 2 m. The stability threshold (± 2 mm/yr) for each dataset has been decided considering the standard deviation of the LOS velocity. This range is also coherent with various literature examples in which C- and X-band InSAR data analysis were used to study subsidence areas of Italy (Tosi et al., 2013; Del Ventisette et al., 2015; Bianchini et al., 2015; Solari et al., 2018).

3.3. Geotechnical data

In order to study the subsurface geological framework of the study area, a series of available on-site survey data were used, including: 13 boreholes (between 36 and 70 m), 32 dilatometer tests (DMT, between 40 and 25 m) and 26 piezocone penetration tests (CPT, between 40 and 30 m). The location of these investigations is reported in Fig. 5. These investigations have been performed between 1992 and 1998 for the construction of the freight terminal. Moreover, several undisturbed samples were collected during the subsurface tests in order to perform some geotechnical investigations for the identification of the main physical and mechanical characteristics of the subsurface soils. When possible, the following geotechnical parameters have been determined: grain size, specific weight (γ), friction angle (φ'), undrained cohesion (c_u), elastic modulus (E), oedometer modulus (E_{oed}), coefficient of consolidation (c_v), coefficient of secondary consolidation (c_α), Plastic limit (PL), Liquid limit (LL), Plasticity Index (PI), Natural water content (W) and Liquidity Index (LI). Subsurface and geotechincal data were used as input to model the settlement induced by the building load using the software Rocscience Settle^{3d} (2009). The obtained model

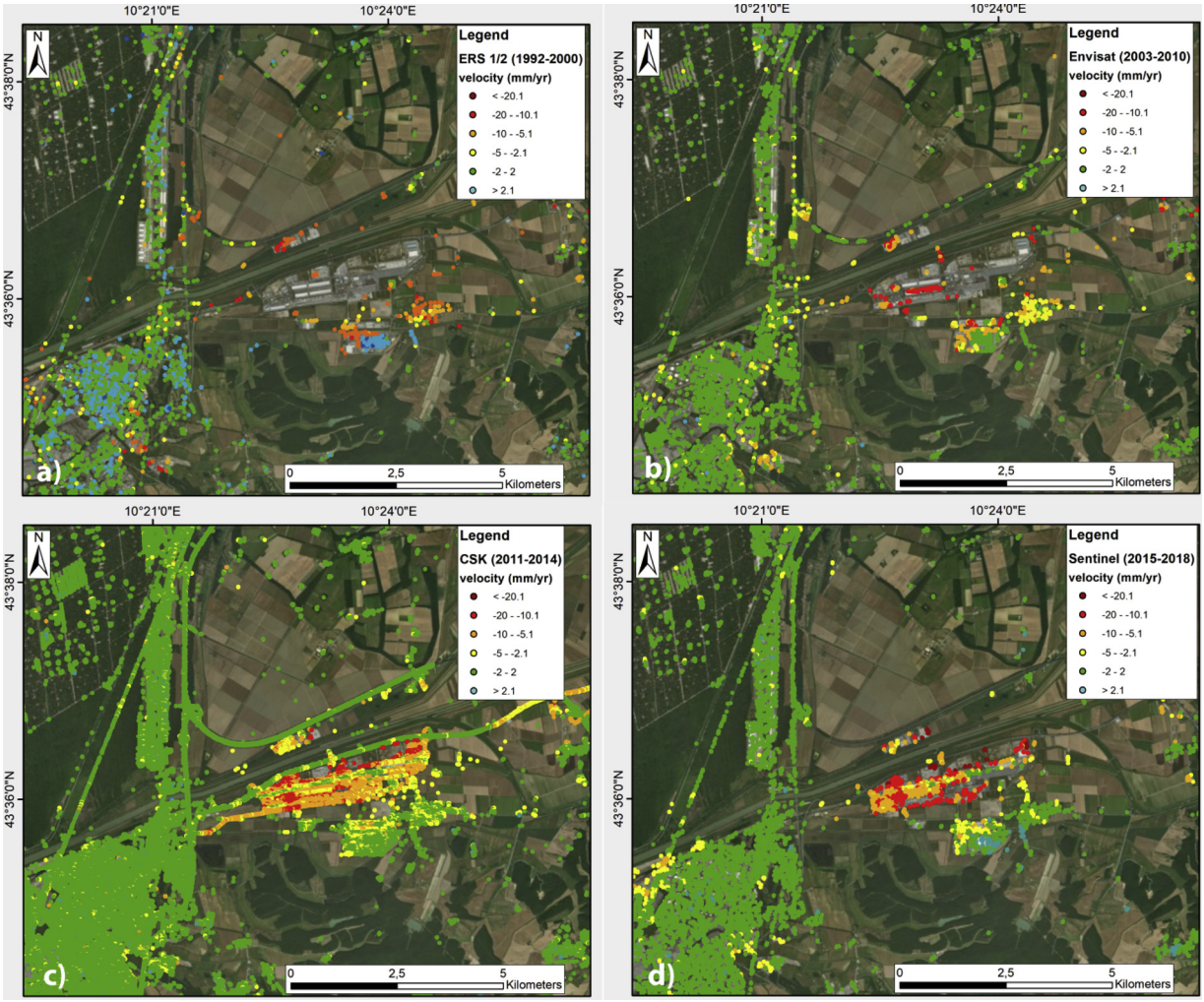

Fig. 4. Ground LOS deformation velocity maps of the study area in different periods of observation: a) ERS 1/2; b) Envisat; c) COSMO-SkyMed; d) Sentinel-1.

allowed to identify the maximum depth at which the building load affects the consolidation process and to evaluate its timing. The consolidation curve was compared to the time series and used to validate InSAR results.

4. Results

4.1. Buildings map

One hundred buildings have been mapped through the analysis of the optical imagery inside the area of the freight terminal. The map highlights that 18 buildings were present when ERS 1/2 started to acquire images, 10 buildings were built between 1992 and 2001, but most of the recognized buildings (65% of the total) were built during the Envisat acquisition period. During the COSMO-SkyMed acquisition period only 3 buildings were added, and others 4 buildings were built during the acquisition period of Sentinel-1 (2015–2018) (Fig. 6). The oldest buildings are located in the southern sector of the freight terminal. The central sector is characterized by warehouses with very similar structures.

4.2. Building deformation maps

The building deformation map extracted from ERS 1/2 (1992–2001) data has allowed measuring the LOS deformation velocity of only 18 buildings (Table 4, Fig. 7a). The buildings for which it was possible to measure the average deformation rate are mostly located in the southern sector of the study area. These buildings, which were also present in the 1954 image, are characterized by a positive LOS velocity (2.7 mm/yr), very close to the stability threshold. The ERS 1/2 building deformation map shows that 11 buildings are characterized by subsidence. The highest velocities (-20.7 mm/yr) have been recorded in the northern (along the right bank of the Scolmatore channel) sector (Fig. 7a).

The period of acquisition of Envisat corresponds with the maximum development of the urbanization of the study area. The derived building deformation map allows us to measure the LOS deformation velocity of 47 buildings (Table 4, Fig. 7b). It is worth noting that the oldest buildings appear as stable or their deformation rate is decreased. On the contrary, the new buildings are characterized by very high LOS velocity (up -20.4 mm/yr, Fig. 7b).

Thanks to its higher resolution, COSMO-SkyMed allows measuring the LOS deformation velocity of most of the buildings (96%) (Table 4, Fig. 7c). CSK map highlights that the deformation rates of those buildings built before the 2011 tend to decrease (e.g. see the line of identical buildings inside the biggest polygon of Fig. 7 which passes from the velocity class < - 20.1 mm/yr to the class -20 < velocity < -10.1), whereas the most recent buildings are characterized by higher LOS deformation velocity (Fig. 7c).

A very similar situation can be seen comparing CSK and Sentinel-1 data (Table 4, Fig. 7d), although the measurement point density is different. The building LOS deformation velocity substantially

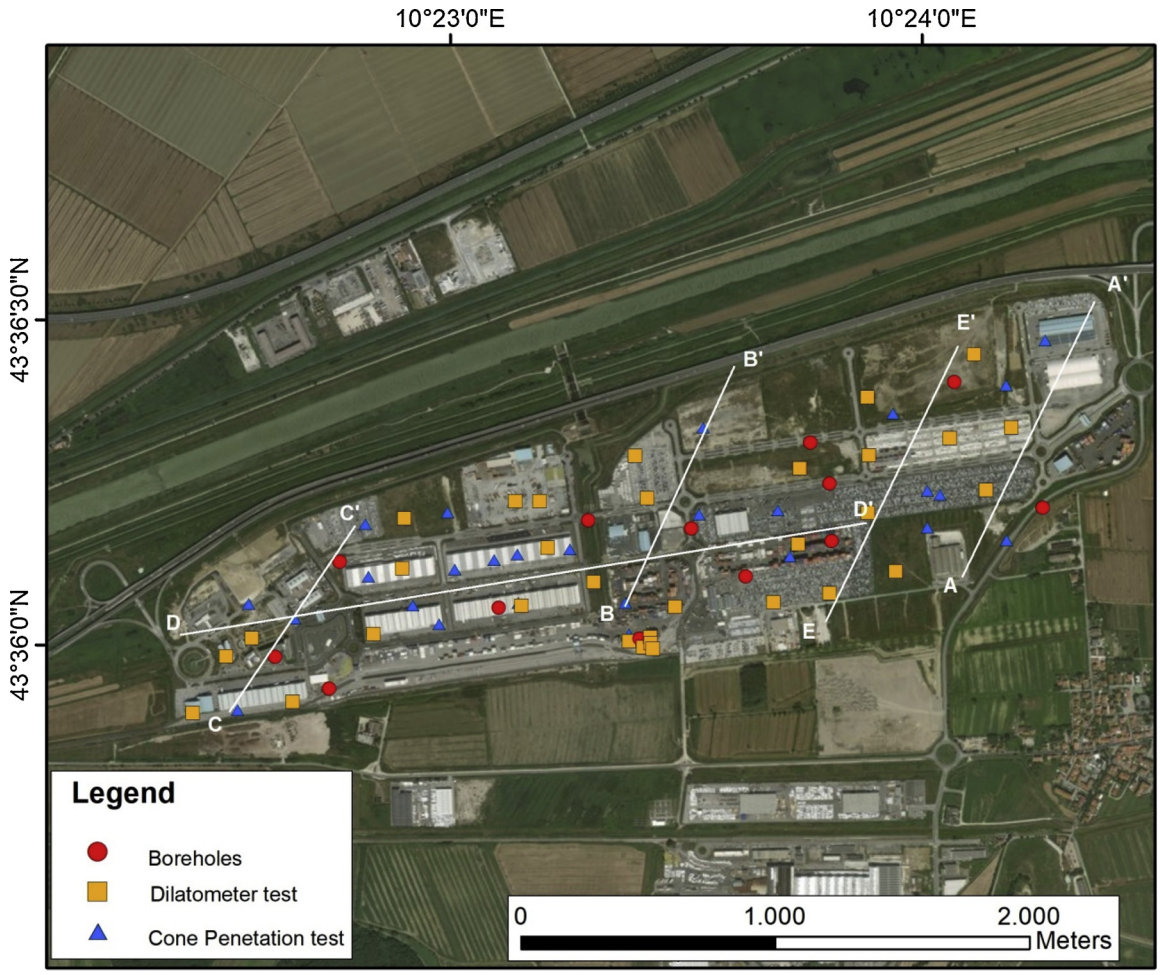

Fig. 5. Location of the on-site investigations and paths of the stratigraphic sections.

decreases for the oldest buildings whereas the highest LOS velocity is detected in correspondence to the most recent ones. In particular, the southern sector is, today, almost completely stable and most of deformation can be recognized in the central sector where the most recent buildings are located (Fig. 7d).

4.3. Time series analysis

The availability of four different satellite datasets covering different periods gave us an unprecedented opportunity to analyze the deformation trend across more than 20 years. Time series analysis has been conducted selecting 5 buildings built in different periods (Figs. 6 and 8, Table 5). The representative time series for each building have been derived by averaging the deformation measured in correspondence with each acquisition of every PS/DS point included in the building boundary. This approximation can be used because no differential deformations have been observed. The gaps between the end of the acquisition of a sensor and the next one were filled by a prediction trendline based on the previous deformation history and considering a linear subsidence trend.

In order to compare the behavior of the ground deformation, the time series of the selected buildings have been plotted in the same graph (Fig. 9). The analysis of the selected time series clearly shows how LOS ground deformation velocities decrease through time for all the buildings and the related trendlines tend to the horizontal. This graph clearly shows how the ground LOS deformation velocity of the most recent buildings is fast with respect to the older ones and how the LOS velocity progressively decrease through time when considering the oldest buildings that record LOS velocities halved passing from ERS 1/2 to Sentinel-1 periods (see for example Building 93 of Fig. 9).

4.4. Geotechnical analysis

The analysis of boreholes, CPT and DMT data allowed to reconstruct in detail the subsurface stratigraphy of the study area (Fig. 10, Table 6). In particular 6 litho-geotechnical units have been recognized and described from top to bottom as follows:

Unit 1: massive brownish clayey silt locally passing to sandy silt. Unit 1 is present in the whole area of the freight terminal with an average thickness of 3.5 m. This unit is characterized by a low friction angle (φ'), high undrained cohesion (c_u) and medium coefficient of consolidation (c_v) (Table 6).

Unit 2: present in the whole area of the freight terminal with an almost homogeneous thickness (˜19 m), maximum in the western sector (22 m) and minimum in the eastern one (15 m). It is made of light gray silty clay with low silty fraction. The clay fraction usually reaches the 70%. The content in organic matter is high (peat, wood fragments). From a geotechnical point of view, it is characterized by a high natural water content (W) that is near to the liquid limit (LL), low φ' and specific weight (γ). The coefficient of consolidation (c_v = 0.63 m^2/yr; Table 6) falls in the range of values typical of the clays of high plasticity (PI > 25% [34]).

Unit 3: represented by thin lenses and/or layers usually interbedded to the units 2 or 4. This unit is made of silty fine sand to coarse sand. In the western sector, the lenses belonging to the unit 3 are located between −8 and −30 m, whereas they are deeper (between −18 and

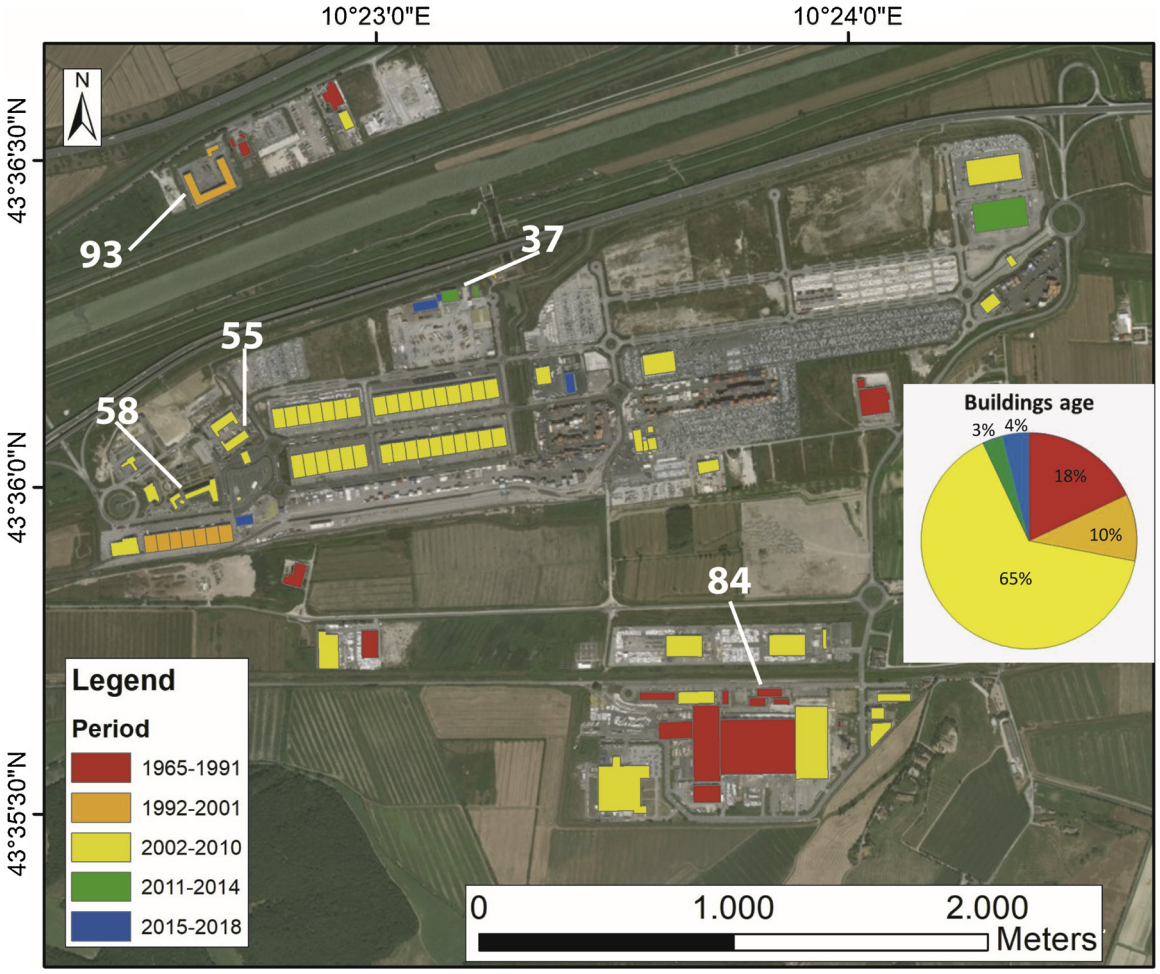

Fig. 6. Building construction map of the freight terminal area inferred by comparing the optical aerial and satellite imagery. The numbers correspond to the buildings the deformation time series of which are presented in the following section. The pie chart shows the percentages of buildings for each class.

Table 4
Statistic of the building LOS deformation velocity map for each SAR sensor.

Velocity interval (mm/yr)	N° of Buildings			
	ERS 1/2	Envisat	CSK	Sentinel-1
> 2.0	3	0	0	1
2.0 - -1.9	4	9	10	21
−2.0 - -4.9	0	3	22	12
−5.0 - -9.9	8	12	41	30
−10.0 - -19.0	3	23	18	12
< −20.0	0	0	5	3
Total Buildings	18	47	96	79
Min velocity	−20.0	−20.0	−35.8	−37.0
Max velocity	2.7	0.2	2.0	2.2

−38 m) in the eastern sector. The geotechnical parameters *LL*, *PL* and *PI* (Table 6) of Unit 3 are mostly related to silty fraction.

Unit 4: made of light gray clayey silt and locally of silty clay with calcareous nodules. Occasionally sandy layers have been observed. This unit shows its maximum thickness (42 m) in the central and eastern sectors of the freight terminal area where several intercalations of Unit 3 have been recognized. In the western sector it is replaced (lateral transition) by the Unit 5. Unit 4 represents the transition between the costal sediments of Unit 5 and the continental deposits located east of the study area. This unit is characterized by high values of *LL* (50) and *PI* (43). As for Unit 2, the c_v value (0.79 m^2/yr) is included in the typical range of the clays of high plasticity.

Unit 5: consists of silty fine to coarse sand with occasional intercalations of few centimeters thick of sandy silt. This unit shows a lateral transition with Unit 4. In the western sector of the study area this unit is present between −32 and −58 m except for 2 small lenses belonging to the Unit 4. In the central part of the study area, Unit 5 is completely lacking and in the eastern part it can be observed between −50 and −52 m.

Unit 6: made of gravel and sandy gravel. The clasts are sub-rounded with diameter ranging from 2 to 4 cm. The thickness of this unit varies between 2 and 5 m; its top is never above 55 m below surface.

The values of oedometer modulus (E_{oed}) of the sediments of units 1, 2 and 4 are that typical of silt and clay of medium-low consistency (Table 6). Moreover, the coefficient of secondary consolidation (c_α) of these sediments vary from 0.0033 to 0.0154 (typical values of normally consolidated clays; Lambe and Whitman, 1979). The worst geotechnical properties mainly characterize the shallowest units (1 and 2) and in particular Unit 2 (Table 6), which is also characterized by larger thickness. Despite the geotechnical features of the clay belonging to Unit 2 were improved by the aging effect, they depreciate when clay is disturbed and remodeled after geotechnical investigations and/or when foundations are built (Tsuchida et al., 1991; Shahriar and Jadid, 2018).

Geotechnical parameters and subsurface stratigraphy were used to model the time -dependent consolidation induced by settle of a warehouse using the software Rocscience Settle 3d (2009) (Fig. 11). The time-dependent consolidation were evaluated after 5, 10, 45 and 100 years for a building of the dimension of building 84 (100 × 30 m). Results show that the most of the consolidation involves unit 2 and,

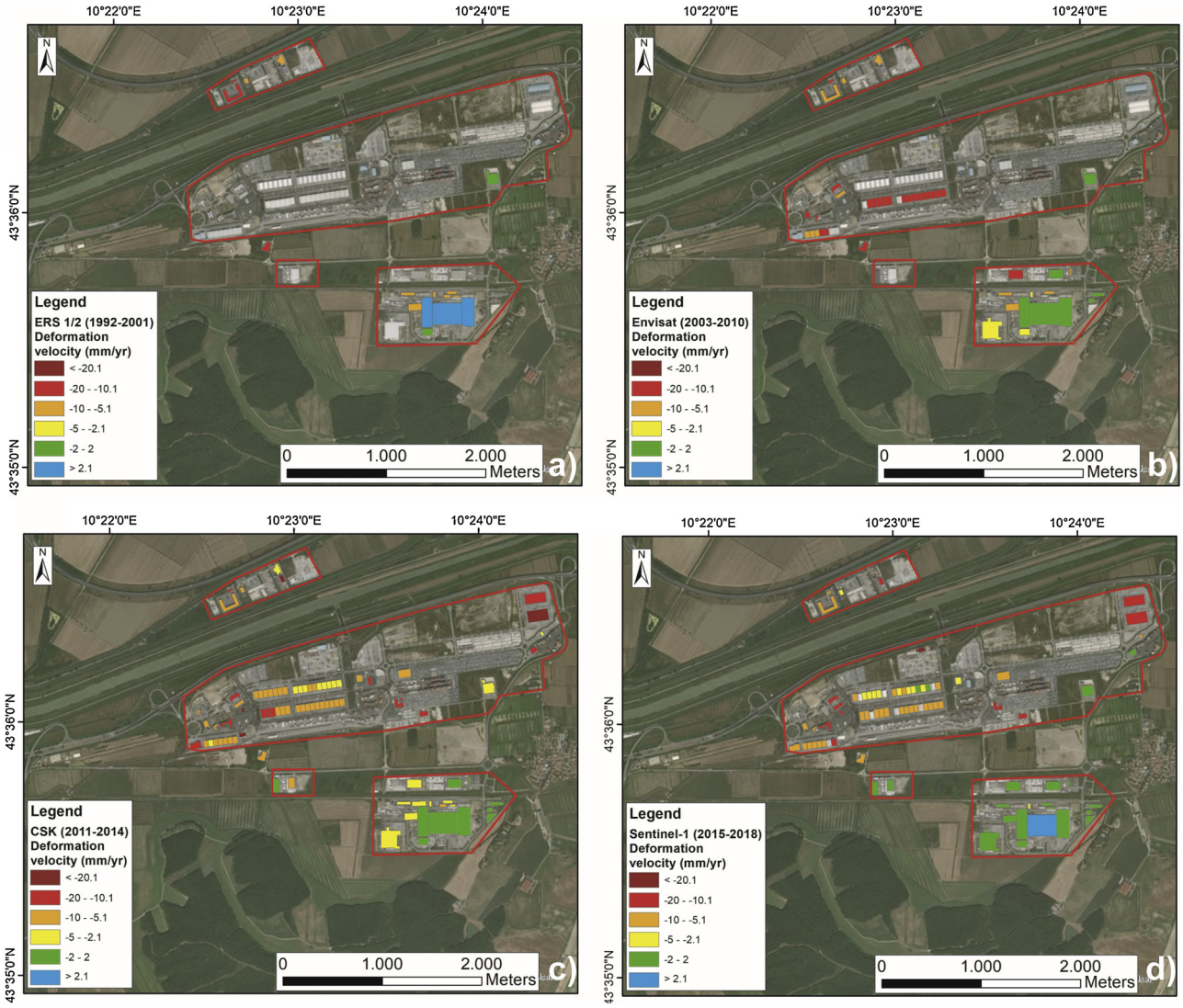

Fig. 7. Building LOS deformation velocity maps in different periods of observation: a) ERS 1/2; b) Envisat; c) COSMO-SkyMed; d) Sentinel-1.

after around 40 years, the settlement bulb reaches also unit 4 (Fig. 11). The deformation induced by the settlement influence an area larger that the building, confirming the need for creating a buffer around each structure when considering PS velocities.

5. Discussion

The subsidence of the study area can be due to different factors: natural (tectonic, natural sediment compaction), or anthropogenic (urbanization or dewatering). Among them, tectonic and natural sediment compaction can be excluded, despite acting today, because of their negligible contribute (− 0.57 mm/yr, Nisi et al., 2003). This value falls inside the accuracy of the PSI method, thus it cannot be measured with sufficient precision with SAR satellite data (Crosetto et al., 2016). Furthermore, despite the study area is located very close to the Livorno-Sillaro fault, the subsidence can be observed only in the neighboring of the freight terminal and not along the rest of the fault. The contribution of shallow Holocene sediment compaction can be excluded as well; this is reasonable considering that the village of Guasticce, 500 m eastern than the freight terminal, lays on the same geological asset of the study area without registering any relevant deformation.

Considering the distribution and magnitude of the LOS velocity measured from 1992, the subsidence affecting the study area must be related to other factors. Groundwater exploitation can be excluded. The area is located few meters below the sea level. The shallow water table is almost stable during the whole year and the resource is of low quality (Garassino, 2002). Furthermore, the subsidence detected using MT-InSAR data is confined in the area of the freight terminal and in case of subsidence related to water extraction the subsidence is usually spread over a more vast area. The analysis of the time series of deformation does not highlight a seasonality related to the water table variation. Moreover, an intense groundwater exploitation is not known in this area. Excluding of tectonics, natural sediments compaction and aquifer exploitation as driven factors of subsidence, the area of Guasticce can be considered as an appropriate test site to understand the effects of man-made loading to land subsidence. In particular, Guasticce is a suitable area for reconstructing the consolidation process of compressible soils induced by the construction of heavy buildings using MTInSAR products. Settlement corresponds with the sum of the imposition of man-made materials to level the ground surface, the construction of primary infrastructures and of buildings (foundation and structure) (Stramondo et al., 2008). More in details, settlement is the combination between the applied load and the mechanic behavior of the loaded soils over time, which is linked also to the fine soil thickness. The settlement is expressed by the primary and the secondary consolidation processes (Terzaghi and Peck, 1967). The primary consolidation is characterized by the greatest settlements which occur in a short period of time. At the beginning of this phase the excess of pore pressure counteracts the increase of the total stress. After a certain time, depending on the hydraulic conductivity of the soil, water tends to be

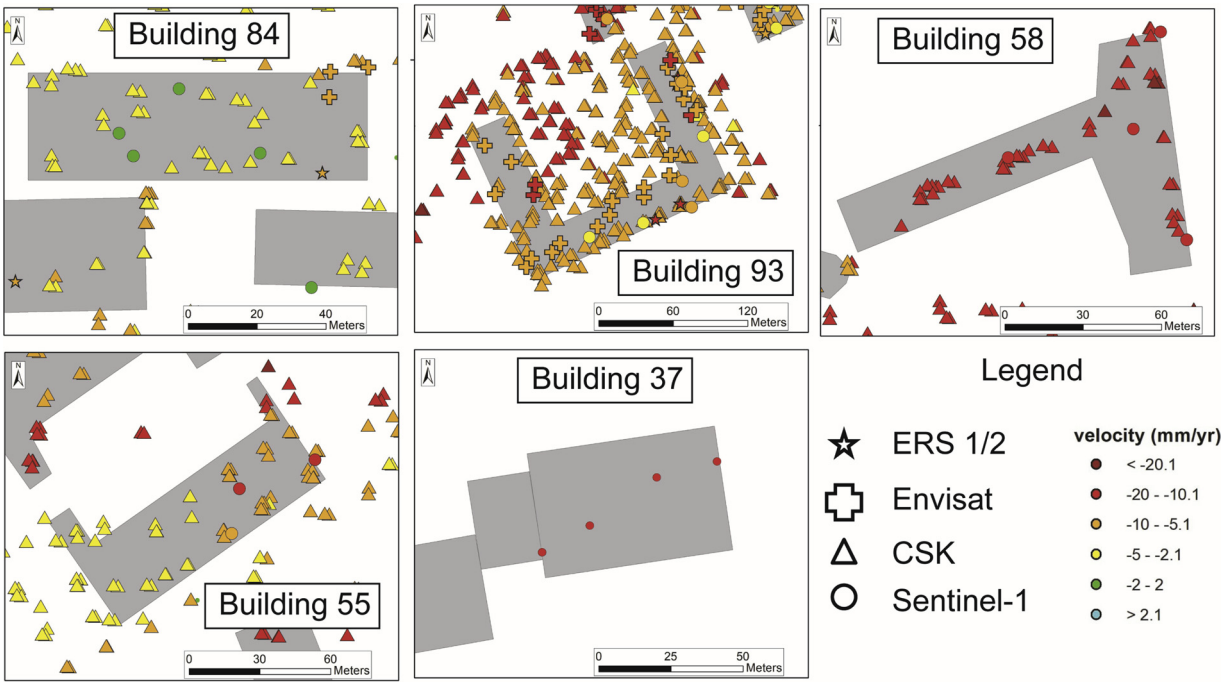

Fig. 8. Building LOS deformation velocity maps of the 5 selected buildings.

Table 5
Measured LOS velocity for the five reference buildings. The age of construction is derived from multi-temporal orthophoto interpretation. For each satellite, the left value represents the number of PS whereas the right number is the average deformation rate (mm/yr).

Building n°	Age of construction	ERS 1/2		Envisat		CSK		Sentinel-1	
84	1965	1	−6.2	4	−5.8	48	−4.2	5	−1.8
93	1996	4	−13.9	35	−8.9	123	−7.2	42	−5.0
58	2003	–		8	−16.1	20	−9.8	10	−8.6
55	2010	–		–		35	−21.7	3	−11.4
37	2013	–		–		–		4	−34.8

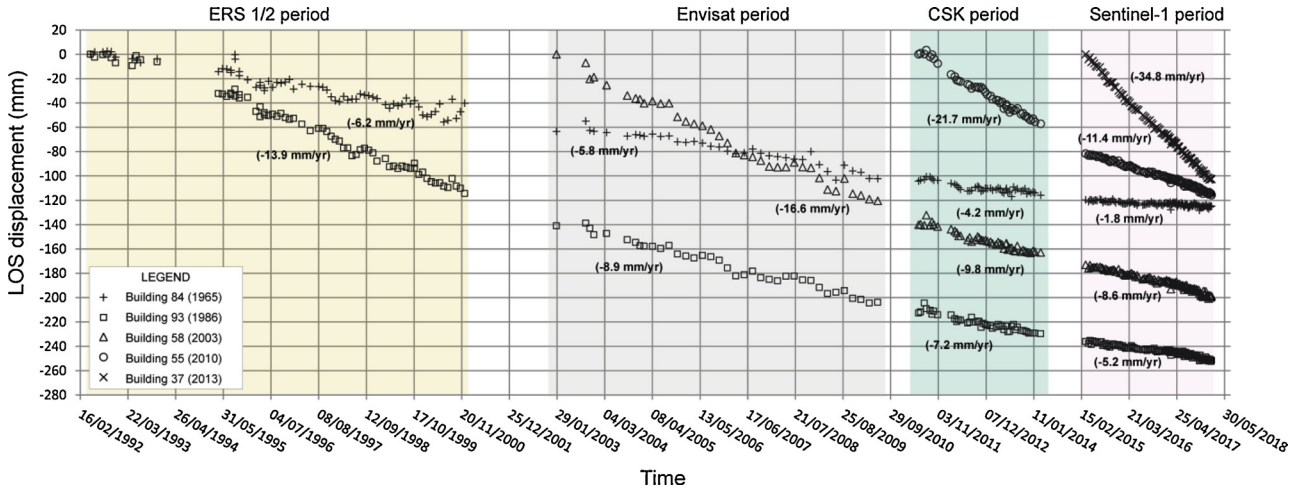

Fig. 9. Comparison among time series of the buildings in different periods.

expelled from the pores and the soil skeleton fully supports the load. The primary consolidation process is, usually, long-lasting in saturated clays because the low permeability delays the dissipation of the excess pore pressure (Kaliakin, 2017). The secondary consolidation occurs at a constant effective stress and it realizes in a longer period. This phase is characterized by a volume change due the presence of, and interaction between, adsorbed water layers in clays (Hansbo, 2015; Kaliakin, 2017). The latter is characterized by low to very low settlement rates and it is related to the viscous behavior of fine-grained and/or organic soils (Fig. 11). The whole process is time-dependent and directly correlated to the type of soil and to its geotechnical and hydrogeological properties (mainly hydraulic conductivity, Terzaghi and Peck, 1967). Considering the example of Fig. 11, the time-dependent consolidation were evaluated (Fig. 12). In this case most of the deformation occurs

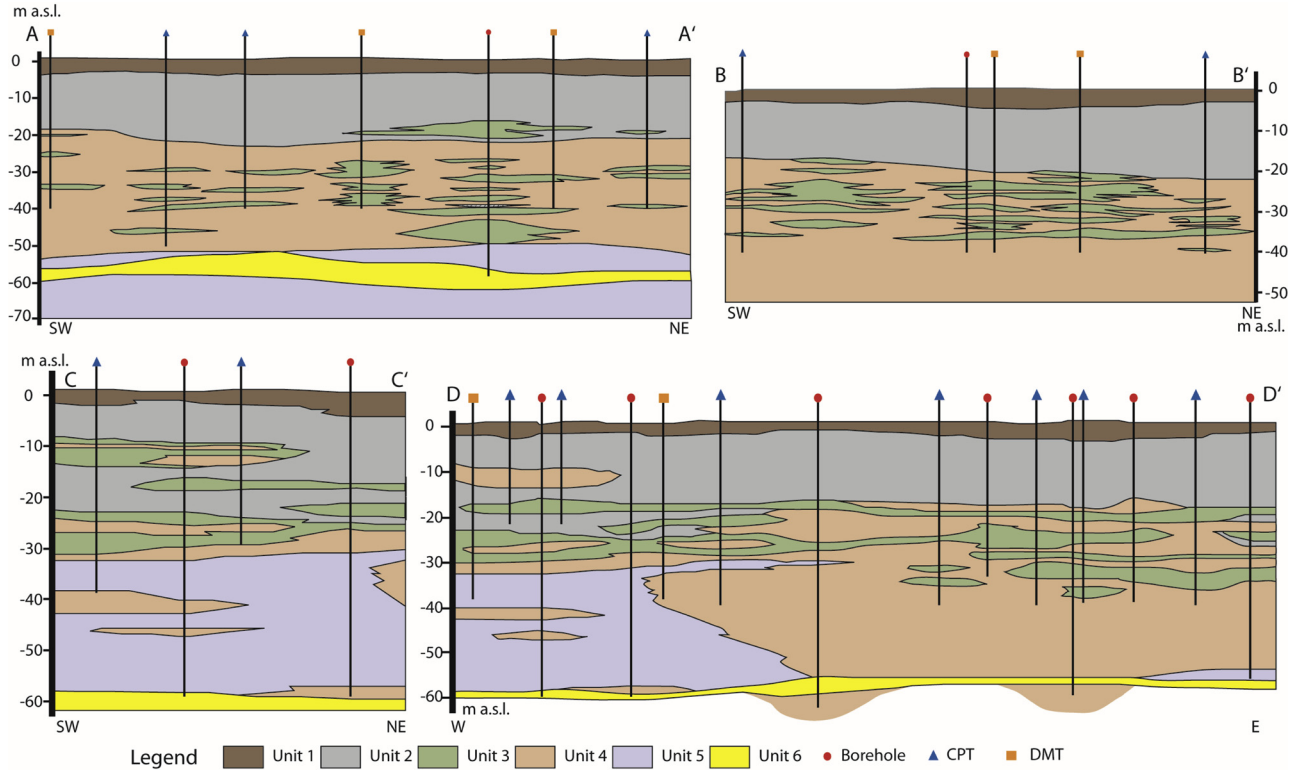

Fig. 10. Stratigraphic section inferred from the subsurface investigations. The paths of the stratigraphic sections appear in Fig. 5.

Table 6
Main geotechnical parameters of the units.1–6.

	Unit 1	Unit 2	Unit 3	Unit 4	Unit 5	Unit 6
γ (kN/m^3)	19	16–16.5	17.5	18.5	19	20
φ' (°)	23–24	21–24	28–33	22–26	30–33	35–37
c_u (kN/m^2)	40–65	12–22	–	23–60	–	–
E (MPa)	–	–	7–15	–	10–12	> 50
E_{oed} (MPa)	5.5–14	1–2.3	10–19	5–8	16	–
c_v (m^2/yr)	1.89	0.63	–	0.79	–	–
LL (%)	65–80	60–80	40–60	50	–	–
PL (%)	30	24–35	20–25	23	–	–
PI (%)	35–50	35–50	15–25	43	–	–
W (%)	39	60	–	–	–	–
LI (-)	0.615	0.7	–	–	–	–

during the first 5 years; in this period the deformation velocity is around 24 mm/yr. After 10 years, the deformation velocity decreases to 15 mm/yr. An important change in the settlement rate occurs around 45 years after the construction, when the deformation rate drop to 5 mm/yr.

The Guasticce area is a valuable test for evaluating the temporal evolution of subsidence induced by the buildings load, in an area characterized by the presence of a 15 m thick layer of compressible clay in its subsurface. The availability of InSAR data acquired during the last 26 years can be exploited in order to understand the timing of the primary and secondary consolidation processes.

Considering the subsidence rates of the selected buildings (Table 5) and the evolution over time (Fig. 9) their settlement can be evaluated.

The building 84, constructed in 1965, is characterized by a deformation rate lower than - 5 mm/yr between 1992 and 2001 and between 2003 and 2010. Starting from the CSK acquisition period (2011–2014), the deformation rates falls down the threshold of - 5 mm/yr. In this case the time series of deformation is very similar to those of Fig. 12 and the change in the curvature of the time series falls around - 5 mm/yr (Fig. 9) suggesting that this velocity can be used to identify the shift between the primary and the secondary consolidation processes. The time series of the rest of the analyzed buildings do not show velocities lower than - 5 mm/yr and they are characterized by a more linear trend without important changes in the curvature.

This means that the primary consolidation process lasted 45 years as confirmed also by the model of Fig. 12. At the moment, it is not possible to evaluate the duration of the secondary consolidation processes because it is still active (Fig. 12). More recent buildings are characterized by subsidence rates lower than - 5 mm/yr, confirming that the primary consolidation processes are still active. In particular, building 93 shows today a subsidence rate of - 5.2 mm/yr, which is very close to the threshold between the primary and secondary consolidation processes after 32 years. The comparison between the velocity measured with satellite data (Table 6) and those obtained by the time-dependent consolidation model (Fig. 12) highlights that InSAR data can be used to evaluate the primary consolidation process. After 5 years the LOS velocity of building 37 is 34.8 mm/yr which is faster than those inferred from the consolidation model (24 mm/yr). The comparison is more refined after 10 years when the difference between model and InSAR results is 3 mm/yr. The consolidation model suggests that around 45 years the deformation velocity is around 5 mm/yr confirming the InSAR results. This assumption can be made considering that the greatest part of the analyzed buildings are sheds with similar constructive characteristics and foundations (raft). The problem related to the presence of a highly compressible clay layer can be also observed in the city of Pisa which is located few km north of the study area (Solari et al., 2017). The Leaning Tower itself is a consequence of high compressibility soil in the subsurface of Pisa (Burland et al., 1998). In the subsurface of Pisa this layer is a little bit deeper and less thick with respect to that of Guasticce. In Pisa, subsidence induced by the soft clay layer is well known since the Middle Age but the reduced thickness lead to a slower subsidence rate with respect to that measured in Guasticce. In fact, similar buildings in Pisa usually do not show damage, on the contrary most of buildings of the freight terminal are affected by structural damages. This difference can be related to the different

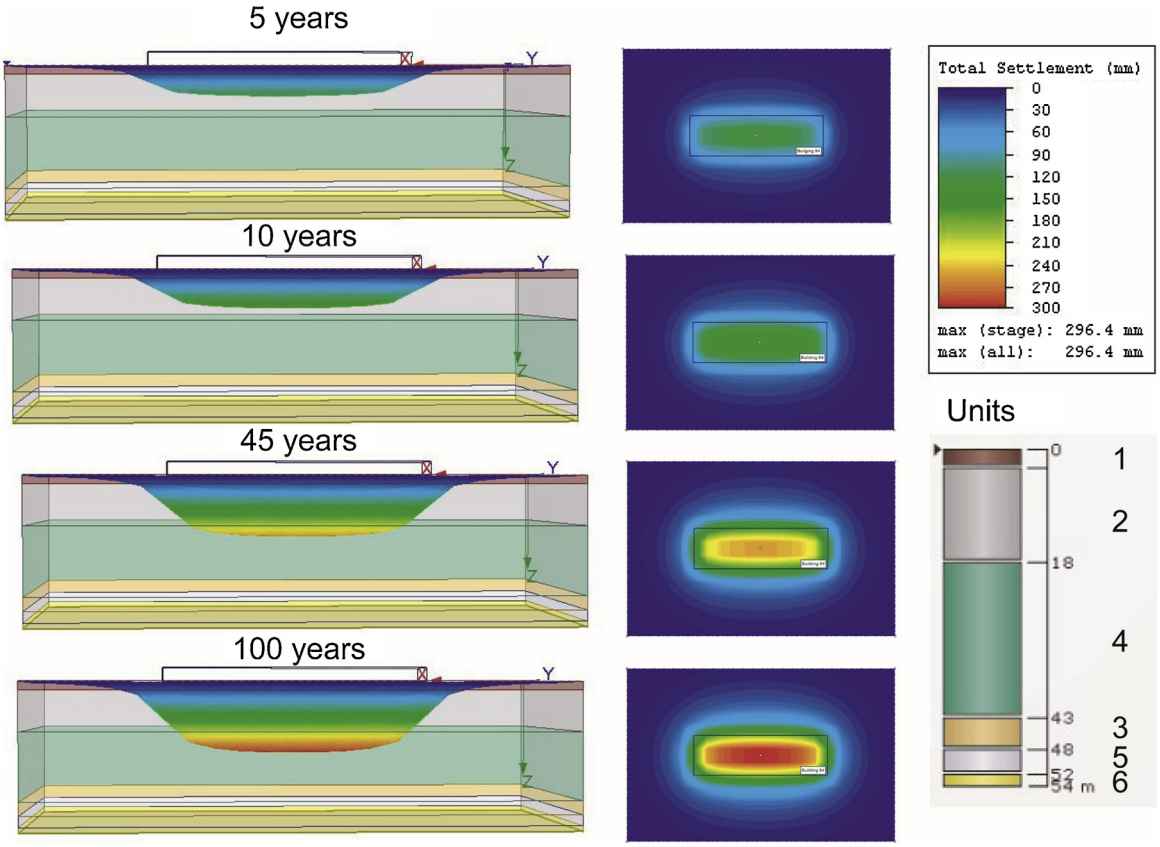

Fig. 11. Model of the deformation induced by the settlement of a warehouse after 5, 10, 45 and 100 years after the construction of the building. On the left: the deformation induced in the subsurface; on the right the deformation in aerial view. The model is calibrated using the subsurface geotechnical data obtained from boreholes.

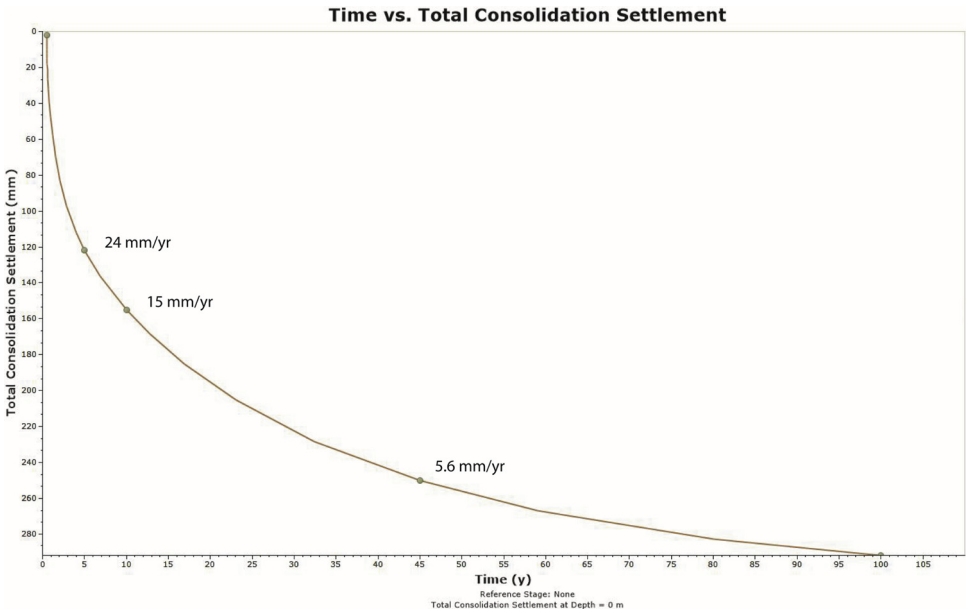

Fig. 12. Consolidation curve derived from the simulation of Fig. 11.

subsidence rates during the primary consolidation phase. In Pisa buildings built in the last 10 years are characterized by rates greater than - 20 mm/yr whereas recent buildings in Guasticce show rates varying between - 20 and - 40 mm/yr.

The importance of the Unit 2 layer in the settlement process is confirmed by the comparison between the deformation rate and the subsurface geological framework. Fig. 13 shows that buildings built during the same period show very similar deformation rates along all the D-D' stratigraphic section despite the stratigraphic structure is different. The only common denominator in the whole area of the freight terminal is represented by Unit 2 which has a significant and constant thickness (15–20 m) and can be considered as the driving factor of the

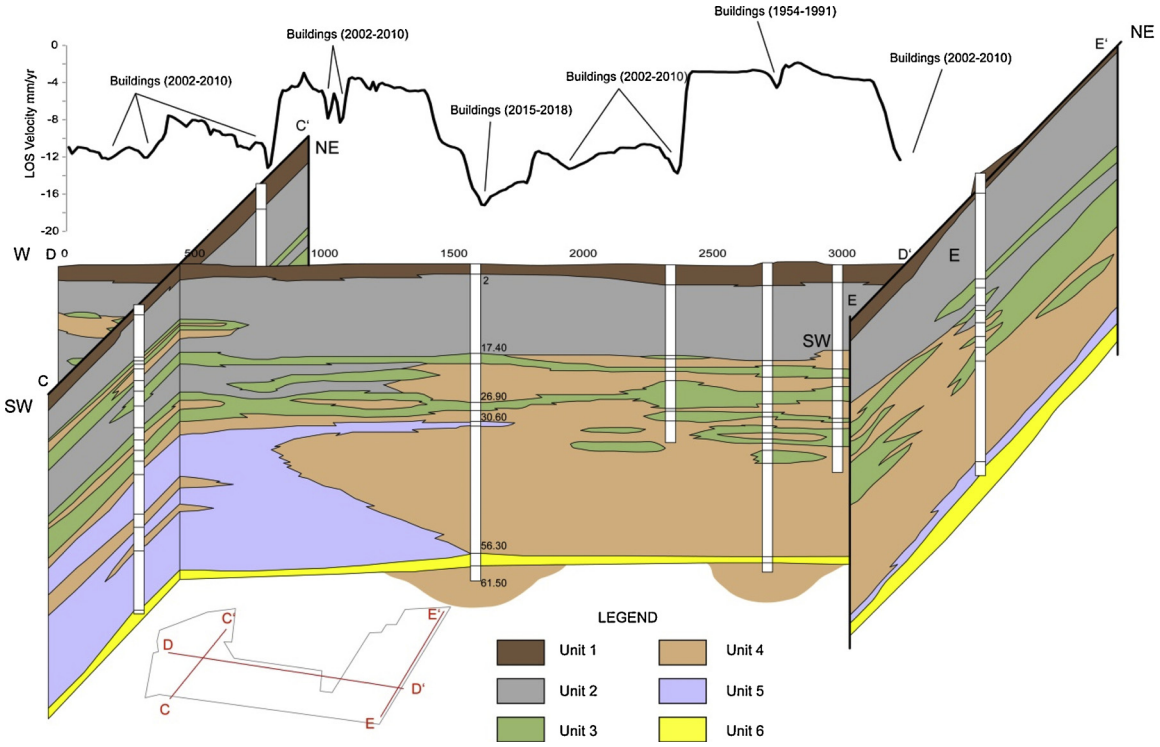

Fig. 13. Comparison between the stratigraphic 3D reconstruction of the freight terminal area and the deformation rate measured with Sentinel-1 data. The line representing the LOS velocity was created by interpolating the PS/DS of Sentinel-1. The bottom figure represents a sketch of the freight terminal.

settlement in the area of the freight terminal.

5. Conclusion

In this study, a very long-term monitoring of the surface deformation using four different sensors has been performed to analyze the settlement induced by the buildings load. The comparison between PSI data and geological/geotechnical data shows that the driving factor of subsidence can be inferred excluding, in this case, tectonics, natural sediment compaction and subsurface water withdrawal.

The analysis of the deformation time series over more than 20 years allowed to identify the timing of the primary and secondary consolidation processes since the deformation rates of single buildings can be accurately measured. The rates are clearly time-dependent from the age of the buildings. In this specific case, a threshold of 5 mm/yr has been decided to separate the primary from the secondary consolidation period. In order to establish a more accurate threshold, more accurate information about building foundations is needed. At the moment, we do not have sufficient data to constrain an accurate model for a complex phenomenon like subsidence. However, it is worth noting that a relationship between the distribution of the subsidence rates and the development of the urbanization of the study area can be observed. This relationship strongly suggests that building loads is the main factor controlling of the subsidence processes within the freight terminal since the rest of the driving factors can be excluded.

In the area of the freight terminal the long-lasting primary consolidation process affects building for around 45 years inducing severe damage. This approach can help in mapping the spatial distribution of poorly consolidated layers in the subsurface of densely urbanized. Therefore, satellite results can help in mapping of this kind of deposits in the subsurface can help in urban planning and in suggesting suitable foundations to avoid structural damage to buildings due to the primary consolidation process.

Author contributions

A. Ciampalini made the overall analysis and interpretation of the data. A. Ciampalini and L. Solari drafted the manuscript and made the study conception and design. S. Moretti supervised the team. R. Giannecchini e Y. Galanti made critical revisions of the paper. All authors discussed the results and provided critical feedback to the manuscript.

Funding

This research was funded by the University of Pisa in the framework of the project PRA_2018_41 “Georisorse e Ambiente”.

Acknowledgement

Constructive comments from two anonymous reviewers and the associate editor improved the manuscript.

References

Aguzzi, M., Amorosi, A., Colalongo, M.L., Ricci Lucchi, M., Rossi, V., Sarti, G., Vaiani, S.C., 2007. Late Quaternary climatic evolution of the Arno coastal plain (Western Tuscany, Italy) from subsurface data. Sed. Geol. 202 (1-2), 211–229.

Armaş, I., Mendes, D.A., Popa, R.G., Gheorghe, M., Popovici, D., 2017. Long-term ground deformation patterns of Bucharest using multi-temporal InSAR and multivariate dynamic analyses: a possible transpressional system? Sci. Rep. 7, 43762.

Bianchini, S., Pratesi, F., Nolesini, T., Casagli, N., 2015. Building deformation assessment by means of persistent scatterer interferometry analysis on a landslide-affected area: the Volterra (Italy) case study. Remote Sens. 7, 4678–4701.

Bianchini, S., Moretti, S., 2015. Analysis of recent ground subsidence in the Sibari plain (Italy) by means of satellite SAR interferometry-based methods. Int. J. Remote Sens. 36, 4550–4569.

Bonano, M., Manunta, M., Pepe, A., Paglia, L., Lanari, R., 2013. From previous C-band to new X-band SAR systems: assessment of the DInSAR mapping improvement for deformation time-series retrieval in urban areas. IEEE Trans. Geosci. Remote Sens. 51 (4), 1973–1984.

Bozzano, F., Esposito, C., Mazzanti, P., Patti, M., Scancella, S., 2018. Imaging Multi-age construction settlement behaviour by advanced SAR interferometry. Remote Sens. 10, 1137.

Bru, G., González, P.J., Mateos, R.M., Roldán, F.J., Herrera, G., Béjar-Pizarro, M., Fernández, J., 2017. A-DInSAR monitoring of landslide and subsidence activity: a case of Urban Damage in Arcos de la Frontera, Spain. Remote Sens. 9 (8), 787.

Bucx, T.H.M., van Ruiten, C.J.M., Erkens, G., de Lange, G., 2015. An integrated assessment framework for land subsidence in delta cities. Proceedings of the International Association of Hydrological Sciences 372, 485–491.

Burland, J.B., Jamiolkowski, M., Viggiani, C., 1998. Stabilising the leaning tower of Pisa. Bull. Eng. Geol. And the Env. 57, 91–99.

Cantini, P., Testa, G., Zanchetta, G., Cavallini, R., 2001. The Plio-Pleistocene evolution of exstensional tectonics in northern Tuscany, as constrained by new gravimetric data from the Montecarlo Basin (lower Arno valley, Italy). Tectonophysics 330, 25–43.

Ciampalini, A., Bardi, F., Bianchini, S., Frodella, W., Del Ventisette, C., Moretti, S., Casagli, N., 2014. Analysis of building deformation in landslide area using multi-sensor PSInSAR technique. Int. J. Appl. Earth Obs. Geoinf. 33, 166–180.

Ciampalini, A., Raspini, F., Frodella, W., Bardi, F., Bianchini, S., Moretti, S., 2016. The effectiveness of high-resolution LiDAR data combined with PSInSAR data in landslide study. Landslides 13, 399–410.

Cigna, F., Lasaponara, R., Masini, N., Milillo, P., Tapete, D., 2014. Persistent scatterer interferometry processing of COSMO-SkyMed StripMap HIMAGE time series to depict deformation of the historic centre of Rome, Italy. Remote Sens. 6 (12), 12593–12618.

Cigna, F., Jordan, H., Batseon, L., McCormack, H., Roberts, C., 2015. Natural and anthropogenic geohazards in Grater London observed from geological and ERS-1/2 and ENVISAT persistent scatterers ground motion data: results from the EC FP7-SPACE PanGeo Project. Pure App, Geophys. 172, 2965–2995.

Costantini, M., Ferretti, A., Minati, F., Falco, S., Trillo, F., Colombo, D., Novali, F., Malvarosa, F., Mammone, C., Vecchioli, F., Rucci, A., Fumagalli, A., Allievi, J., Ciminelli, M.G., Costabile, S., 2017. Analysis of surface deformation over the whole Italian territory by interferometric processing of ERS, Envisat and COSMO-SkyMed radar data. Remote Sens. Environ. 202, 250–275.

Crosetto, M., Monserrat, O., Cuevas-González, M., Devanthéry, N., Crippa, B., 2016. Persistent scatterer interferometry: a review. ISPRS J. Photogramm. Remote Sens. 115, 78–89.

Del Ventisette, C., Solari, L., Raspini, F., Ciampalini, A., Di Traglia, F., Moscatelli, M., Pagliaroli, A., Moretti, S., 2015. Use of the PSInSAR data to map highly compressible soil layers. Geol. Acta 13, 309–323.

Ferretti, A., Prati, C., Rocca, F., 2001. Permanent scatterers in SAR interferometry. IEEE Trans. Geosci. Remote. Sens. 39, 8–20.

Ferretti, A., Fumagalli, A., Novali, F., Prati, C., Rocca, F., Rucci, A., 2011. A new algorithm for processing interferometric data-stacks: SqueeSAR. IEEE Trans. Geosci. Remote. Sens. 49, 3460–3470.

Garassino srl Interporto Toscano Amerigo Vespucci SpA, 2002. Compendio sulle indagini geognostiche effettuate sull'area di Interporto. Technical Report.

Ghelardoni, R., Giannini, E., Nardi, R., 1965. Ricostruzione paleogeografica dei bacini neogenici e quaternari della bassa valle dell'Arno sulla base dei sondaggi e rilievi sismici. Mem. Soc. Geol. It. 7, 91–106.

Hansbo, S., 2015. Chapter 2 – experience of consolidation process from test areas with and without vertical drains. In: Indraratna, Buddhima, Chu, Jian, Rujikiatkamjorn, Cholachat (Eds.), Ground Improvement Case Histories. Butterworth-Heinemann, pp. 33–82. https://doi.org/10.1016/B978-0-08-100192-9.00002-8.

Herrera, G., Tomás, R., Monells, D., Centolanza, G., Mallorquí, J.J., Vicente, F., Navarro, V.D., Lopez-Sanchez, J.M., Sanabria, M., Cano, M., Mulas, J., 2010. Analysis of subsidence using TerraSAR-X data: murcia case study. Eng. Geol. 116 (3-4), 284–295.

Holzer, T.L., Johnson, A.I., 1985. Land subsidence caused by ground water withdrawal in urban areas. GeoJournal 11 (3), 245–255.

Hu, X., Oommen, T., Lu, Z., Wang, T., Kim, J.-W., 2017. Consolidation settlement of Salt Lake County tailings impoundment revealed by time-series InSAR observations from multiple radar satellites. Rem. Sens. Environ. https://doi.org/10.1016/j.rse.2017.05.023. in press.

Jones, C.E., An, K., Blom, R.G., Kent, J.D., Ivins, E.R., Bekaert, D., 2016. Anthropogenic and geologic influences on subsidence in the vicinity of New Orleans, Louisiana. J. Geophys. Res. Solid Earth 121, 3867–3887.

Kaliakin, V.N., 2017. Chapter 8 - example problems related to compressibility and Settlement of soils. In: Kaliakin, Victor N. (Ed.), Soil Mechanics. Butterworth-Heinemann, pp. 331–376. https://doi.org/10.1016/B978-0-12-804491-9.00008-2.

Lambe, T.W., Whitman, R.V., 1979. Soil Mechanics. SI Version. Wiley, New York.

National Cartographic Portal, 2019. National Cartographic Portal. Pst-A Project (*Piano Straordinario di Telerilevamento*). http://www.pcn.minambiente.it/viewer/.

Nisi, M.F., Antonioli, F., Dai Pra, G., Leoni, G., Silenzi, S., 2003. Coastal deformation between the Versilia and the Garigliano plains (Italy) since the last interglacial stage. J. Quat. Sci. 18 (3), 709–721.

Peduto, D., Nicodemo, G., Maccabiani, J., Ferlisi, S., 2017. Multi-scale analysis of settlement-induced building damage using damage surveys and DInSAR data: a case study in the Netherlands. Eng. Geol. 218, 117–133.

Pratesi, F., Tapete, D., Terenzi, G., Del Ventisette, C., Moretti, S., 2015. Rating healt and stability of engineering structures via classification indexes of InSAR Persistent Scatterer. Int. J. Appl. Earth Obs. Geoinf. 40, 81–90.

Pratesi, F., Tapete, D., Del Ventisette, C., Moretti, S., 2016. Mapping interactions between geology, subsurface resources exploitation and urban development in transforming cities using InSAR Persistent Scatterer: two decades of change in Florence, Italy. App. Geogr. 77, 20–37.

Raspini, F., Bianchini, S., Ciampalini, A., Del Soldato, M., Solari, L., Novali, F., Del Conte, S., Rucci, A., Ferretti, A., Casagli, N., 2018. Continuous, semi-automatic monitoring of ground deformation using Sentinel-1 satellites. Sci. Rep. 8. https://doi.org/10.1038/s41598-018-25369-w.

Rocscience Inc, 2009. Settle 3d Version 2.0 - Settlement/Consolidation Analysis. Rocscience Inc., Toronto, Ontario, Canada. www.rocscience.com.

Sarti, G., Rossi, V., Giacomelli, S., 2015. The Upper Pleistocene "Isola di Coltano sands" (Arno coastal plain, Tuscany, Italy): review of stratigraphic data and tectonic implications for the southern margin of the Viareggio Basin. Atti Soc. Tosc. Sc. Nat. Serie A 122, 75–84.

Shahriar, A.R., Jadid, R., 2018. An experimental investigation on the effect of thixotropic aging on primary and secondary compression of reconstituted dredged clays. Appl. Clay Sci. https://doi.org/10.1016/j.clay.2018.05.023.

Shirzaei, M., Bürgmann, R., 2018. Global climate change and local land subsidence exacerbate inundation risk to the San Francisco Bay Area. Sci. Adv. 4 (3). https://doi.org/10.1126/sciadv.aap9234.

Solari, L., Ciampalini, A., Raspini, F., Bianchini, S., Moretti, S., 2016. PSInSAR analysis in the Pisa urban Area (Italy): a case study of subsidence related to stratigraphical factors and urbanization. Remote Sens. 8 (2), 120.

Solari, L., Ciampalini, A., Raspini, F., Bianchini, S., Zinno, I., Bonano, M., Manunta, M., Moretti, S., Casagli, N., 2017. Combined use of C-and X-Band SAR data for subsidence monitoring in an urban area. Geosciences 7 (2), 21.

Solari, L., Del Soldato, M., Bianchini, S., Ciampalini, A., Ezquerro, P., Montalti, R., Raspini, F., Moretti, S., 2018. From ERS 1/2 to Sentinel-1: subsidence monitoring in Italy in the last two decades. Front. Earth Sci. 6 (149). https://doi.org/10.3389/feart.2018.00149.

Stramondo, S., Bozzano, F., Marra, F., Wegmuller, U., Cinti, F.R., Moro, M., Saroli, M., 2008. Subsidence induced by urbanisation in the city of Rome detected by advanced InSAR technique and geotechnical investigations. Remote Sens. Environ. 112 (6), 3160–3172.

Tosi, L., Teatini, P., Strozzi, T., 2013. Natural versus anthropogenic subsidence of Venice. Sci. Rep. 3, 2710.

Terzaghi, K., Peck, R.B., 1967. Soil Mechanics in Engineering Practice. John Wiley & Sons.

Tsuchida, T., Kobayashi, M., Mizukami, J.-I., 1991. Effect of aging of marine clay and its duplication by high tempature consolidation. Soils Found. 31, 133–147.

Zhou, X., Chang, N.B., Li, S., 2009. Applications of SAR interferometry in earth and environmental science research. Sensors 9 (3), 1876–1912.

Zhu, M., Wan, X., Fei, B., Qiao, Z., Ge, C., Minati, F., Vecchioli, F., Li, J., Costantini, M., 2018. Detection of building and infrastructure instabilities by automatic spatio-temporal analysis of satellite SAR interferometry measurements. Remote Sens. 10 (11), 1816.